

See discussions, stats, and author profiles for this publication at: <https://www.researchgate.net/publication/231680660>

Synthesis and Characterization of Carboxylate-Modified Gold Nanoparticle Powders Dispersible in Water

ARTICLE *in* LANGMUIR · JANUARY 1999

Impact Factor: 4.46 · DOI: 10.1021/la9812828

CITATIONS

290

READS

45

2 AUTHORS, INCLUDING:



Keisaku Kimura

Hosei University

186 PUBLICATIONS 3,749 CITATIONS

SEE PROFILE

Synthesis and Characterization of Carboxylate-Modified Gold Nanoparticle Powders Dispersible in Water

Sihai Chen and Keisaku Kimura

Department of Material Science, Faculty of Science, Himeji Institute
of Technology, Harima Science Garden City, Kamigori,
Hyogo 678-1297, Japan

Langmuir®
The ACS Journal of Surfaces and Colloids

Reprinted from
Volume 15, Number 4, Pages 1075–1082

Synthesis and Characterization of Carboxylate-Modified Gold Nanoparticle Powders Dispersible in Water

Sihai Chen and Keisaku Kimura*

*Department of Material Science, Faculty of Science, Himeji Institute of Technology,
Harima Science Garden City, Kamigori, Hyogo 678-1297, Japan*

Received September 17, 1998. In Final Form: December 1, 1998

Carboxylate-modified gold nanoparticles have been synthesized in a single-phase system based on the reduction of hydrogen tetrachloroaurate(III) by sodium borohydride in methanol using mercaptosuccinic acid (MSA) as the stabilizing thiol ligand. Five samples with diameters of 10.2, 10.8, 12.8, 19.4, and 33.6 Å have been prepared as water-redispersible powders through decreasing the initial MSA/HAuCl₄ molar ratio from 2.5 to 0.5. These samples were characterized by X-ray diffraction, transmission electron microscopy, elemental analysis, thermogravimetric analysis, ζ -potential measurement, Fourier transform infrared spectroscopy, and UV-vis spectroscopy. The results show that a large number of the particles are fcc single crystals with the polyhedral morphology of a truncated octahedral motif and that a self-assembled monolayer of thiolates has indeed formed through the adsorption of mercapto groups on the gold particle surface; the maximum packing density of the thiolates is 15.23 Å² per mercapto group. The surface structures of the powders are clearly defined; MSA on the particle surface exists in the form of sodium carboxylate, and one MSA unit combines with one H₂O molecule.

Introduction

The synthesis of colloidal gold has been studied intensively for a long time.¹ Recently, a method developed by Brust et al.² for the generation of long chain alkanethiolate-stabilized gold nanoparticles has caused extensive interest due to the superb stability of the particles; they are easily dispersible in organic solvent and can be reisolated as pure powders. Following this finding, much work has been done to modify the properties such as reactivity and solubility of the nanoparticles through changing the molecular structures of the thiolates on the particle surface.^{3–9} This includes the use of long chain thiolates containing an aromatic moiety,³ ω -substituted (cyano, bromo, vinyl, ferrocenyl)⁴ and poly-hetero- ω -functionalized⁵ long chain alkanethiolates, as well as small molecular thiolates such as (γ -mercaptopropyl)trimethoxysilane⁶ and the rigid aromatic thiols of 4-mercaptopbiphenyl⁷ and p -mercaptophenol.⁸ A recent work also showed that sodium 3-mercaptopropionate can be used for the synthesis of gold nanoparticles using citrate as reductant;⁹ however, since this method was applied in diluted aqueous solution (the total concentration of HAuCl₄ ~5 × 10⁻⁴ M), it is difficult to separate the particles as solid powders, preventing the detailed characterization of the surface

structure with a variety of methods where solid powders are needed as the specimens.

In this report, we describe a new method for the large-scale synthesis of carboxylate-modified gold nanoparticle powders using mercaptosuccinic acid (MSA) as the stabilizer. We will also describe the characterization of thus prepared particles with a variety of methods such as X-ray diffraction, transmission electron microscopy, elemental analysis, thermogravimetric analysis, Fourier transform infrared spectroscopy, UV-vis spectroscopy, and ζ -potential measurement. Special emphasis is focused on the elucidation of the surface structure of these particles. A striking feature of the carboxylate-modified gold nanoparticles is that they are easily dispersible in water, a property that has not been achieved using other kinds of thiolates.^{2–8} This implies that they will find important use in the field of immunogold cytochemistry–histochemistry, where water dispersibility is a prerequisite for being used as an immunocytochemical marker in electron microscopy because the particles should combine with macromolecules in living or fixed cells or tissues in aqueous solution.¹ Furthermore, since the gold particles prepared here can be precipitated with poor solvent and redispersed in water without aggregation, we can easily narrow the size distribution with the size-selective precipitation techniques.^{10,11} This makes them extremely attractive compared to the other aqueous gold colloids, which often suffer the problem of easy aggregation and cannot be prepared in concentrated solutions.¹² In addition, the size of carboxylate-modified particles can be easily tuned to as small as 1 nm, making them an excellent candidate as marker in cell–biological electron microscopy studies.

The successful large-scale generation of carboxylate-modified gold particles implies the possibility to assemble the nanoparticles into large artificially designed nano-

* Corresponding author. Fax: 81-7915-8-0161. Telephone: 81-7915-8-0159. E-mail: kimura@sci.himeji-tech.ac.jp.

(1) *Colloidal Gold: Principles, Methods and Applications*; Hayat, M. A., Ed.; Academic Press: San Diego, CA, 1989; Vols. 1 and 2.

(2) Brust, M.; Walker, M.; Bethell, D.; Schiffrin, D. J.; Whymann, R. *J. Chem. Soc., Chem. Commun.* 1994, 801–802.

(3) Johnson, R. S.; Evans, S. D.; Mahon, S. W.; Ulman, A. *Langmuir* 1997, 13, 51–57.

(4) Hostetler, M. J.; Green, S. J.; Stokes, J. J.; Murray, R. W. *J. Am. Chem. Soc.* 1996, 118, 4212–4213.

(5) Ingram, R. S.; Hostetler, M. J.; Murray, R. W. *J. Am. Chem. Soc.* 1997, 119, 9175–9178.

(6) Buining, P. A.; Humbel, B. M.; Philipse, A. P.; Verkleij, A. J. *Langmuir* 1997, 13, 3921–3926.

(7) Brown, L. O.; Hutchison, J. E. *J. Am. Chem. Soc.* 1997, 119, 12384–12385.

(8) Brust, M.; Fink, J.; Bethell, D.; Schiffrin, D. J.; Kiely, C. J. *J. Chem. Soc., Chem. Commun.* 1995, 1655–1656.

(9) Yonezawa, T.; Sutoh, M.; Kunitake, T. *Chem. Lett.* 1997, 619–620.

(10) Murray, C. B.; Norris, D. J.; Bawendi, M. G. *J. Am. Chem. Soc.* 1993, 115, 8706–8715.

(11) Vossmeye, T.; Katsikas, L.; Giersig, M.; Popovic, I. G.; Diesner, K.; Chemseddine, A.; Weller, H. *J. Phys. Chem.* 1994, 98, 7665–7673.

(12) Handley, D. A. In *Colloidal Gold: Principles, Methods and Applications*; Hayat, M. A., Ed.; Academic Press: San Diego, CA, 1989; Vol. 1, pp 13–32.

structures through hydrogen-bonding interaction¹³ or charge-charge interaction.¹⁴ Since molecules with the carboxylic acid functional group have been widely used to form large self-assembled architectures in supramolecular chemistry,^{15–17} it is reasonable to suppose that the stable gold particles covered with carboxylate groups can also be used as units for generating two- or three-dimensional nanocrystal superlattices or for the hybridized self-assembling between supramolecular architectures and nanoparticles. This implies great potential for new material creation, which will be useful in electronics and optics.^{18–20} At present, an overwhelming method for nanocrystal superlattice formation is through hydrophobic interaction, that is, through the modification of particles with long chain hydrocarbon compounds.^{21–32} To this end, the particles prepared here may predict a new method of nanocrystal superlattice formation if monodispersed carboxylate-covered gold nanoparticles were used.

Experimental Section

Chemicals. The following reagents were all used as received: from Wako Pure Chemical Co., hydrogen tetrachloroaurate tetrahydrate ($\text{HAuCl}_4 \cdot 4\text{H}_2\text{O}$, 99%), mercaptosuccinic acid ($\text{HOOCCH}_2\text{CH}(\text{SH})\text{COOH}$, 97%), methanol (99.8%), ethanol (99.5%), and other organic solvents which are all of reagent grade; from Merck Chemical Co., sodium borohydride (NaBH_4 , >96%). Distilled water of high resistivity (>18.0 M Ω cm) was obtained from an Advantec GS-200 aquarius automatic water distillation supplier.

Particle Preparation. Gold particles of 10.2–33.6 Å diameter were synthesized by changing the MSA/HAuCl₄ molar ratio with a fixed concentration of HAuCl₄. For a typical preparation of 10.2 Å particles, 0.5 mmol of HAuCl₄ dissolved as a 5% (w/v) aqueous solution was at first mixed with 1.25 mmol of MSA in 100 mL methanol to give a transparent solution in a 500-mL Erlenmeyer flask. A freshly prepared 0.2 M aqueous sodium

- (13) Cusack, L.; Rizza, R.; Gorelov, A.; Fitzmaurice, D. *Angew. Chem., Int. Ed. Engl.* **1997**, *36*, 848–851.
- (14) Giersig, M.; Mulvaney, P. *J. Phys. Chem.* **1993**, *97*, 6334–6336.
- (15) Philp, D.; Stoddart, J. F. *Angew. Chem., Int. Ed. Engl.* **1996**, *35*, 1154–1196.
- (16) Decher, G. In *Comprehensive Supramolecular Chemistry*; Sauvage, J. P., Hosseini, M. W., Eds.; Elsevier Science: Oxford, 1996; Vol. 9, 507–528.
- (17) Fredericks, J. R.; Hamilton, A. D. In *Comprehensive Supramolecular Chemistry*; Sauvage, J. P., Hosseini, M. W., Eds.; Elsevier Science: Oxford, 1996; Vol. 9, pp 565–594.
- (18) Special issue of *Phys. Today* **1993**, *46* (6), 22–73.
- (19) Kumar, A.; Whitesides, G. M. *Science* **1994**, *263*, 60–62.
- (20) Asher, S. A.; Holtz, J.; Liu, L.; Wu, Z. *J. Am. Chem. Soc.* **1994**, *116*, 4997–4998.
- (21) Andres, R. P.; Bielefeld, J. D.; Henderson, J. I.; Janes, D. B.; Kolagunta, V. R.; Kubiak, C. P.; Mahoney, W. J.; Osifchin, R. G. *Science* **1996**, *273*, 1690–1693.
- (22) Motte, L.; Billoudet, F.; Pileni, M. P. *J. Phys. Chem.* **1995**, *99*, 16425–16429.
- (23) Motte, L.; Billoudet, F.; Lacaze, E.; Douin, J.; Pileni, M. P. *J. Phys. Chem. B* **1997**, *101*, 138–144.
- (24) Taleb, A.; Petit, C.; Pileni, M. P. *Chem. Mater.* **1997**, *9*, 950–959.
- (25) Taleb, A.; Petit, C.; Pileni, M. P. *J. Phys. Chem. B* **1998**, *102*, 2214–2220.
- (26) Murray, C. B.; Kagan, C. R.; Bawendi, M. G. *Science* **1995**, *270*, 1335–1338.
- (27) Ohara, P. C.; Leff, D. V.; Heath, J. R.; Gelbart, W. M. *Phys. Rev. Lett.* **1995**, *75*, 3466–3469.
- (28) Reetz, M. T.; Winter, M.; Tesche, B. *J. Chem. Soc., Chem. Commun.* **1997**, 147–148.
- (29) Whetten, R. L.; Khouri, J. T.; Alzarez, M. M.; Murthy, S.; Vezmar, I.; Wang, Z. L.; Stephens, P. W.; Cleveland, C. L.; Luedtke, W. D.; Landman, U. *Adv. Mater.* **1996**, *8*, 428–433.
- (30) Heath, J. R.; Knobler, C. M.; Leff, D. V. *J. Phys. Chem. B* **1997**, *101*, 189–197.
- (31) Sato, T.; Brown, D.; Johnson, B. F. G. *J. Chem. Soc., Chem. Commun.* **1997**, 1007–1008.
- (32) Harfenist, S. A.; Wang, Z. L.; Alzarez, M. M.; Vezmar, I.; Whetten, R. L. *J. Phys. Chem.* **1996**, *100*, 13904–13910.

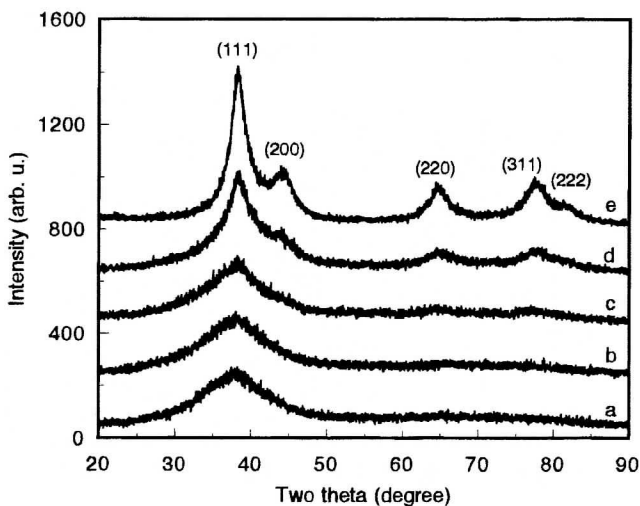


Figure 1. X-ray diffraction patterns of gold particles. The average size and the initial S/Au molar ratio used during preparations are as follows: (a) 10.2 Å, 2.5; (b) 10.8 Å, 2.0; (c) 12.8 Å, 1.5; (d) 19.4 Å, 1.0; (e) 33.6 Å, 0.5. The diffraction patterns were offset vertically for clarity.

borohydride solution (25 mL) was then added at a rate of 5 mL per min under vigorous stirring. The solution turned dark-brown immediately but remained transparent until approximately 13 mL of the reductant was added. The pH of the solution during this process increased gradually from 1.5 to 5.0. Further addition of the reductant resulted in a flocculent dark-brown precipitate, and finally the pH of the solution was brought to 8.6. After further stirring for 1 h, the solvent was removed by decantation after the centrifugation force of 9840g (corresponding to 10000 rpm with the centrifuge used) for 5 min. The precipitate was washed twice with a 20% (v/v) water/methanol solution through an ultrasonic redispersion–centrifugation process to remove the inorganic (Na, Cl, B) or organic impurities. This process was further repeated with 99.8% methanol to remove unbound MSA or Au–MSA complexes. At last, the precipitate was suspended in ethanol and dried by rotary evaporation without exceeding a temperature of 40 °C, followed by evacuating on a vacuum line (<5 × 10⁻³ Torr) for a further 12 h, giving 128 mg of powder.

Instrumentation and Characterization. X-ray diffraction (XRD) was performed on a Rigaku Rint 2000 diffractometer with Cu K α radiation ($\lambda = 1.5418$ Å) operated at 40 kV and 20 mA. The size of the gold nanoparticles was estimated according to the broadening of the full width at half-maximum (fwhm) of the (111) diffraction peak by Scherrer's equation.³³ The fwhm of the (111) diffraction peak was estimated with a least-squares fitting method by assuming that model functions for (111) and (200) peak profiles can be expressed as Lorentzian functions. A bulk gold film with thickness > 3000 Å on a glass mount prepared by vacuum evaporation was used as the reference to correct for the “instrumental broadening” effect.

A Hitachi-8100 transmission electron microscope (TEM), operated at 200 kV with 2.1 Å point-to-point resolution, was used to size and analyze the particles. The specimen was prepared by dropping gold nanoparticles dispersed in 10% (v/v) aqueous ethanol solution on the amorphous carbon-coated copper microgrids and letting them dry in a vacuum line (<5 × 10⁻³ Torr) for 12 h and then keeping them in a drybox with a relative humidity < 20%. For observing the particles shown in Figure 3, a beryllium metal-coated copper microgrid was used. The size distributions were obtained by treating the digitized photo image with a NIH Image 1.61 software package. The high-resolution digitized images with atomic resolutions were enlarged through an Image Intensifier ($\times 20$) and recorded in a Macintosh computer.

Fourier transform infrared (FT-IR) spectra were measured with a Horiba FT-210 infrared spectrophotometer using a 150 mg KBr disk dispersed with the gold powder or MSA solid at a

(33) Warren, B. E. *X-ray Diffraction*; Constable and Company: U.K., 1990; Chapter 13.

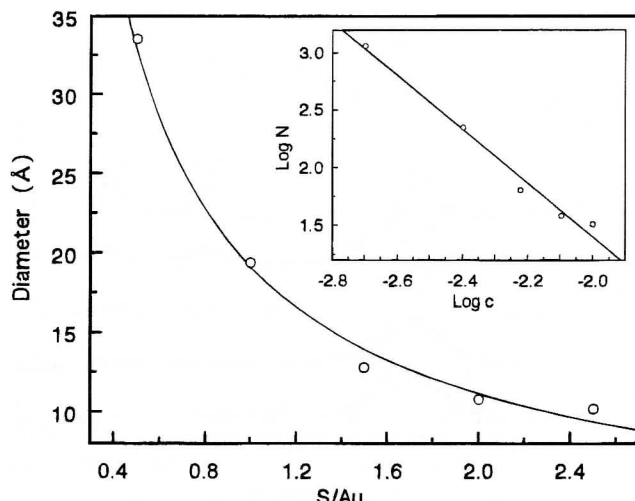


Figure 2. Relationship between the mean diameters of gold nanoparticles and the initial S/Au molar ratios. The inset shows a double-logarithmic plot of the number of atoms in a gold particle versus the concentration of MSA.

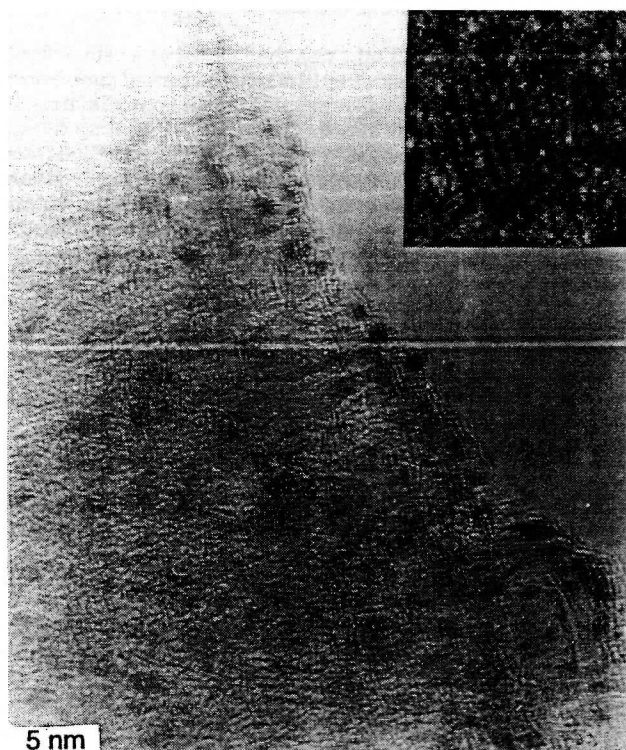


Figure 3. Electron microscopic image of gold particles prepared with the S/Au ratio 2.5. The well-separated particles can be clearly seen near the edge of the microgrid. The average size and standard deviation of the particles were estimated to be 1.2 ± 0.28 nm. The inset shows one particle with seven clearly visible (111) lattice planes.

fixed weight ratio of 0.4%. The background correction was made using a reference "blank" KBr pellet.

Elemental analyses of C, H, O, S, Au, and Na were conducted commercially at the chemical microanalytical laboratory of the Institute of Physical and Chemical Research, Japan, using standard techniques. Specifically, Au and Na were analyzed by atomic absorption spectroscopy. For accuracy, all the analysis was conducted at least twice. Elemental analyses of the residues of gold samples after heating were carried out with a Kevex EDAX analyzer attached to the Hitachi-8100 TEM system.

Thermogravimetry and differential thermoanalysis (TG/DTA) were performed on a fully computerized MAC 2000S system (MAC Sci. Co.) at a heating rate of 10 °C/min in the temperature range

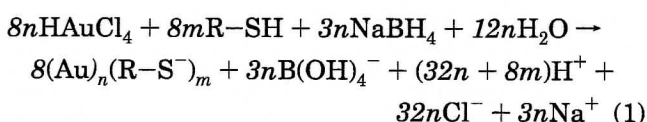
24–499 °C under a nitrogen flow of 40 mL/min. The sampling time was 4 s. Approximately 10 mg of the sample was analyzed with 10.23 mg of Al₂O₃ powder as the reference in standard aluminum pans.

UV-vis absorption spectra of the samples were recorded on a Hitachi U-3210 spectrophotometer in the range 200–900 nm with 2 nm resolution. Quartz cuvettes with a 1-cm optical length were used.

ζ -Potential and dynamic light scattering measurements were performed with an Otsuka ELS 800 electrophoretic light-scattering instrument with a 10-mW He-Ne laser as the light source. The dynamic size of 5 nm to 5 μ m of the particles or their aggregates can be determined.

Results and Discussion

Synthesis and Properties. The synthesis of gold particles was conducted by direct chemical reduction of chloroauric acid in the presence of MSA in methanol in order to simultaneously control the growth of the particle nuclei and attach the self-assembled MSA monolayer on the nuclei surface. The overall reaction can be written as follows (MSA = R-SH):



The initial molar ratio between MSA and chloroauric acid, denoted as S/Au ($=m/n$), was adjusted to control the relative rates of particle nucleation and growth. This parameter finally determined the particle size.

Although H⁺ ions were released in reaction 1, the final pH of the reaction mixture increased with the addition of NaBH₄ (see Experimental Section); this is due to the strong hydrolysis of NaBH₄:



Thus the final pH is determined by the combination of reactions 1 and 2. If a smaller amount of MSA (corresponding to a lower S/Au ratio) is added, the final pH will be higher. For example, the final pH of the reaction solution of 19.4-Å particles (S/Au = 1.0) and 10.2-Å particles (S/Au = 2.5) is found to be 9.3 and 8.6, respectively. Note that, during the addition of NaBH₄, the dispersibility of gold particles abruptly decreased when the pH of the solution increased to around 5. Since the pK_{a1} and pK_{a2} values of succinic acid are, respectively, 4.19 and 5.64,³⁴ it shows the particle precipitation is related to the change of the carboxylic acid to its carboxylate ion form. This evidence indicates that MSA has indeed been derivatized on the gold particle surface. Due to these pH-dependent properties, gold particles can be easily separated from inorganic and organic impurities by increasing the pH of the solution, as we have done during the preparation. This property was further confirmed by the following control experiment: the gold powder in methanol can be dispersed as a transparent dispersion after the addition of a small amount of a 1 M hydrochloric acid solution. Further addition of a 1 M aqueous sodium hydroxide solution resulted in precipitate again.

The gold particles are not suspended in organic solvents such as methanol, ethanol, 2-propanol, acetone, dimethyl sulfoxide, dimethylformamide, pyridine, tetrahydrofuran, and acetonitrile but are easily dispersible in neutral water. This property is notable, since till now gold nanoparticles were only found to be dispersible in alkaline aqueous

(34) Wade, L. G., Jr. *Organic Chemistry*; Prentice Hall: New York, 1987; p 978.

solution ($\text{pH} \geq 13$) using other kinds of thiolate such as *p*-mercaptophenol.⁸ Another feature of our gold particles lies in that the dispersibility of the powder in water is size-dependent; that is, it increases as the particle size decreases (e.g. larger than 10 mg/mL for the 10.2-Å particle and 2 mg/mL for the 19.4-Å particle, respectively). This can be best viewed as a result of the increase in the relative number ratio of MSA molecules to the gold atoms in the smaller particles. Assuming that the gold particles are spherical with radius R and removing an outer shell of gold atoms from the particle results in a change in R of 2.38 Å; the relative ratio of the surface gold atoms to the total atoms is about 85% and 57% for the 10.2-Å and 19.4-Å particles, respectively. Supposing the occupation densities of thiolates on the gold surface are the same, the relative number ratio of MSA molecules to the gold atoms is almost 1.5 times in the former case, resulting in a larger dispersibility.

Size and Inner Structure of Particles. Figure 1 shows the XRD patterns for five samples prepared with different initial S/Au molar ratios. It was found that the particle sizes (estimated from Scherrer's equation) decreased with the increase in S/Au ratios. This result is similar to that reported by Leff et al. for the long chain alkylthiol passivated gold nanoparticles,³⁵ suggesting that the thermodynamics are responsible for the particle stability. The typical diffraction peaks which belong to fcc gold can be clearly observed for the particle whose diameter ≥ 2 nm (Figure 1 d and e). However, for the smaller particles only a broad (111) peak was discernible (Figure 1a–c). The relationship between the particle sizes and the initial S/Au ratios was displayed in Figure 2. As can be seen in the inset, a straight line was found for the double-logarithmic plot of the number of atoms in a gold particle,³⁶ N , versus the MSA concentration, c (M). It obeys the relationship

$$\log N = a - b \log c \quad (3)$$

with $a = -3.25$ and $b = 2.33$. This means the aggregation number of gold atoms decreased with the 2.33th power of the MSA concentration. This power is more than two times higher than that we found in a similar relationship when AgI nanoparticles were formed in aqueous solution in the presence of thiolate.³⁷ It is about six times higher than that in the case of CdS: when CdS nanoparticles were stabilized with thiols in THF solvent, the aggregation number decreased with the power of 0.36–0.42th of the thiolate concentration.³⁸ It shows that thiolate is more efficient in terminating the growth of gold particles than it is in the case of a semiconductor such as CdS or AgI.

Quantitative size information can be obtained with a TEM. The particles prepared with $S/\text{Au} = 2.5$ have an average diameter of 1.2 nm (Figure 3), which is similar to that estimated from the XRD peak broadening method (10.2 Å), suggesting that most of the particles are single crystals. This result is supported by the high-resolution image, as displayed for one particle in the inset of Figure 3; seven clearly visible (111) lattice planes of gold ($d_{111} = 2.35$ Å) covered the whole particle. The well-recognizable near-1-nm particles can only be observed using carefully dried specimens (evacuated for several days in a vacuum

(35) Leff, D. V.; Ohara, P. C.; Heath, J. R.; Gelbart, W. M. *J. Phys. Chem.* **1995**, *99*, 7036–7041.

(36) Calculated from the mean diameter of the particle, supposing the density of gold is 59 atom/nm³.

(37) Chen, S.; Ida, T.; Kimura, K. *J. Phys. Chem. B* **1998**, *102*, 6169–6176.

(38) Fischer, C. H.; Henglein, A. *J. Phys. Chem.* **1989**, *93*, 5578–5581.

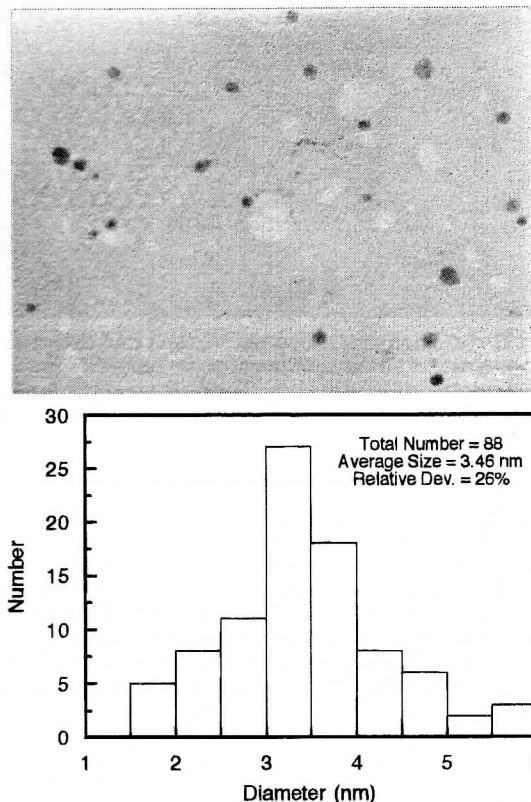


Figure 4. Electron microscopic image and size distribution of gold particles prepared with the S/Au ratio 0.5.

line). Otherwise, even under very weak electron beam irradiation, the particles severely aggregated into larger ones. Several investigators have reported the structural instability of the 1–3-nm particles due to the electron beam irradiation.^{39–42}

Larger particles prepared with smaller S/Au ratios are more stable for TEM observation. Figure 4 shows the photodistribution and size distribution of the particles prepared with an S/Au ratio of 0.5. The average size of 3.46 nm is in good agreement with that calculated from Scherrer's equation (3.36 nm). High-resolution transmission electron microscopy revealed that a large number of the particles can be viewed with clear (111) lattice fringes covering the whole particle if optimum defocus was chosen, showing that these particles are single fcc crystals. Figure 5 a shows one of these particles with polyhedral morphology. As schematically shown in Figure 5b, it belongs to the family of the truncated-octahedral (TO) motif and is defined as the TO⁺ structure with the indices (2,6). The detailed TO structural motif concept has been thoroughly discussed in the case of long chain thiolate-modified gold particles.²⁹ The particle sizes measured parallel to the [100] and [111] directions are respectively 2.6 and 2.7 nm, which are in good agreement with those from theoretical prediction.

The optical spectra of gold particles in aqueous solution are shown in Figure 6. A continuous rising background toward higher energy can be seen for all the samples, which is due to the Mie scattering from the nanoparticle suspension. For the particles smaller than 2 nm (Figure

(39) Iijima, S.; Ichihashi, T. *Phys. Rev. Lett.* **1986**, *56*, 616–619.

(40) Smith, D. J.; Petford-Long, A. K.; Wallenberg, L. R.; Bovin, J. O. *Science* **1986**, *233*, 872–875.

(41) Ajayan, P. M.; Marks, L. D. *Phys. Rev. Lett.* **1989**, *63*, 279–282.

(42) Mitome, M.; Tanishiro, Y.; Takayanagi, K. *Z. Phys. D* **1989**, *12*, 45–51.

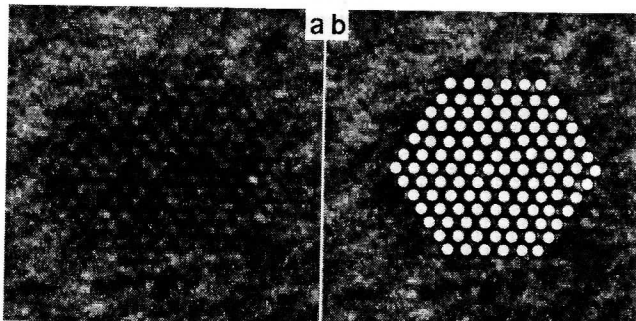


Figure 5. (a) High-resolution micrograph and (b) schematic atomic diagram of the lattice image of one particle from Figure 4 viewed from the [110] direction. The distances between lattice planes are $d_{111} = 2.35 \text{ \AA}$ and $d_{200} = 2.03 \text{ \AA}$ (vertical direction in the figure).

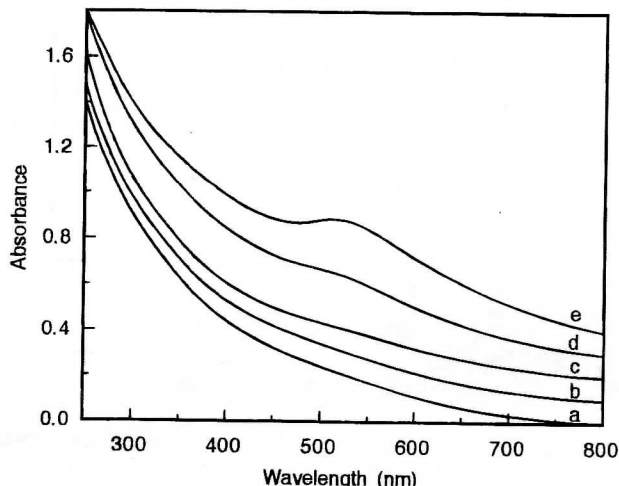
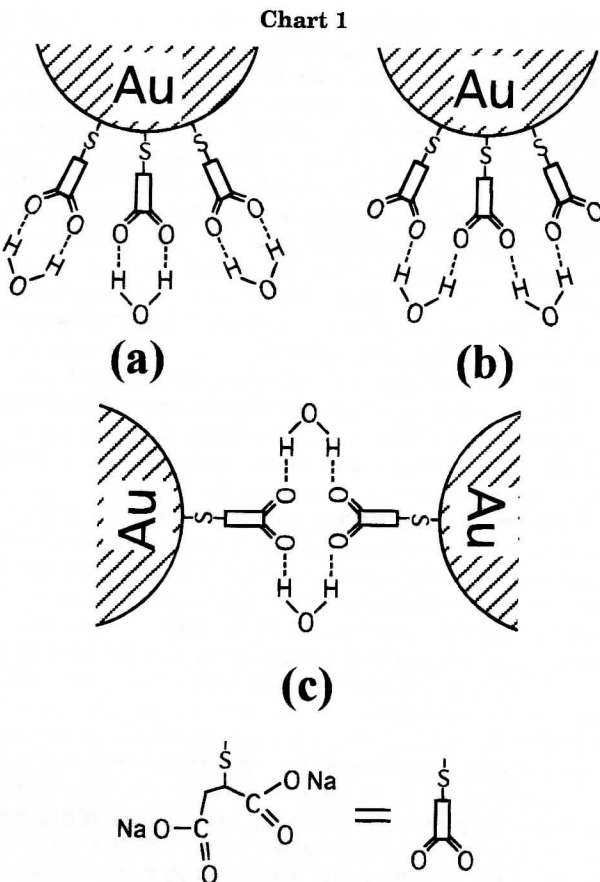


Figure 6. UV-vis spectra of the Au particles with different sizes: (a) 10.2 \AA ; (b) 10.8 \AA ; (c) 12.8 \AA ; (d) 19.4 \AA ; and (e) 33.6 \AA . The spectra are normalized arbitrarily at 800 nm and offset vertically. The solutions are all made in distilled water with the concentration $86 \mu\text{g/mL}$.

6a–c), orange-brown solutions are observed, and no additional absorption peak appears around 500 nm . This is consistent with what has already been observed for smaller gold clusters with a similar size.^{43,44} When the particle size increases to 19.4 \AA (Figure 6d), superimposed on the background, a broad surface plasmon band around 500 nm which is ascribed to a collective oscillation of conduction electrons in response to optical excitation⁴⁵ begins to appear. This band becomes more apparent for the particles with average size 33.6 \AA (Figure 6e). This result is consistent with that of a recent optical study using long chain thiolate-modified gold nanoparticles in the size range from 1.4 to 3.2 nm , which shows the surface plasmon band is essentially unidentifiable for crystallites of less than 2.0 nm effective diameter.⁴⁶

Surface Structure of Particles. To clearly learn the structures of organics on the particle surface, elemental analysis of the 10.2-\AA sample was conducted twice for accuracy. The result was as follows (in %): C, 8.13; H, 0.85; O, 14.07; S, 5.88; Au, 60.74; Na, 8.15. The summation of all the elements amounts to 97.32%, showing that other



impurities such as B and Cl are not present in a significant amount. This also confirmed that the purification steps during preparation were successful. The apparent molecular formula of the particles can be written as $\text{C}_{4.04}\text{H}_{5.06}\text{O}_{5.23}\text{SAu}_{2.02}\text{Na}_{2.11}$. Compared with that of MSA, supposing that it adsorbs on the gold surface through the mercapto group and exists in the form of a sodium carboxylate ($\text{C}_4\text{H}_5\text{O}_4\text{SNa}_2$), one molecular H_2O was found to combine with one MSA unit. It is most probable that the H_2O molecule combines with carbonyl groups in the MSA molecule through a hydrogen-bonding interaction. One H_2O molecule can connect with either two carbonyl groups in one MSA molecule or two carbonyl groups in adjoining MSA molecules on one particle making a successive hydrogen-bonding network, as shown in parts a and b of Chart 1. Another manner of combination is that the water molecule connects with two carbonyl groups from different particles, as shown in part c of Chart 1. In this case, the water molecule acts as “glue” to connect two neighbor particles.

Since the surface structure shown in Chart 1 is deduced from the analysis of 10.2-\AA particles, in the following we will see whether this structure can be applied to other sized particles. According to the structures of Chart 1, the theoretical weight percentages of Au, Na, H_2O , and organics for different sized particles can be calculated. These were then compared with that measured from atomic absorption spectroscopy and thermogravimetric analysis (Table 1). In the theoretical calculation, the total weight can be expressed as $W = W_{\text{Au}} + W_{\text{Na}} + W_{\text{H}_2\text{O}} + W_{\text{org}}$; thus, the weight percentage of Au (P_{Au}), Na (P_{Na}), H_2O ($P_{\text{H}_2\text{O}}$), and organics (P_{org}) can be expressed as $P_{\text{Au}} = W_{\text{Au}}/W$, $P_{\text{Na}} = W_{\text{Na}}/W$, $P_{\text{H}_2\text{O}} = W_{\text{H}_2\text{O}}/W$, and $P_{\text{org}} = W_{\text{org}}/W$. Supposing that the gold particle has the diameter D , then $W_{\text{Au}} = 6W_{\text{Au}}M_{\text{Au}}/dDS_0N_0$, $W_{\text{Na}} = 12W_{\text{Au}}M_{\text{Na}}/dDS_0N_0$, $W_{\text{H}_2\text{O}} = 6W_{\text{Au}}M_{\text{H}_2\text{O}}/dDS_0N_0$, and $W_{\text{org}} = 6W_{\text{Au}}M_{\text{org}}/dDS_0N_0$, where

(43) Fauth, K.; Kreibig, U.; Schmid, G. *Z. Phys. D* **1989**, *12*, 515–520.

(44) Duff, D. G.; Baiker, A.; Edwards, P. P. *J. Chem. Soc., Chem. Commun.* **1993**, 96–98.

(45) Mulvaney, P. *Langmuir* **1996**, *12*, 788–800.

(46) Alzarez, M. M.; Khouri, J. T.; Schaaff, T. G.; Shafiqullin, M. N.; Vezmar, I.; Whetten, R. L. *J. Phys. Chem. B* **1997**, *101*, 3706–3712.

Table 1. Weight Percentages (in %) of Au, Na, H₂O, and Organics Obtained from Atomic Absorption Spectroscopy and Thermogravimetric Analysis for Different Sized Particles

particle diameter (Å)	atomic absorption spectroscopy		thermogravimetric analysis		predicted content of organics ^b
	Au	Na	H ₂ O	organics ^a	
10.2	60.7	8.2	3.8	11.8	27.3
10.8	61.0	6.9	2.3	10.8	30.0
12.8	63.8	6.8	2.3	11.2	27.3
19.4	72.0	5.9	2.5	9.0	19.9
33.6	80.6	2.9	1.7	5.7	14.8

^a Obtained according to the mass loss during the heating process.

^b Obtained by subtraction those of Au, Na, and H₂O from 100%.

d is the bulk density of gold (19.3 g/cm³), *S*₀ is the occupation area of thiolate on gold, *N*₀ is Avogadro's constant, and *M* is the molecular weight. Finally, we can get the theoretical weight percentage of different components:

$$P_{\text{Au}} = dDS_0N_0/[dDS_0N_0 + 6(2M_{\text{Na}} + M_{\text{H}_2\text{O}} + M_{\text{org}})] \quad (4)$$

$$P_{\text{Na}} = 12M_{\text{Na}}/[dDS_0N_0 + 6(2M_{\text{Na}} + M_{\text{H}_2\text{O}} + M_{\text{org}})] \quad (5)$$

$$P_{\text{H}_2\text{O}} = 6M_{\text{H}_2\text{O}}/[dDS_0N_0 + 6(2M_{\text{Na}} + M_{\text{H}_2\text{O}} + M_{\text{org}})] \quad (6)$$

$$P_{\text{org}} = 6M_{\text{org}}/[dDS_0N_0 + 6(2M_{\text{Na}} + M_{\text{H}_2\text{O}} + M_{\text{org}})] \quad (7)$$

The weight percentages are functions of the particle diameter *D*. When using a typical packing density of *S*₀ = 21.4 Å² for the thiolate self-assembling on a flat gold plane,^{47,48} we cannot get a good fit between theoretical and experimental values for all the components. An example is given for the content of gold, shown as the bold line in Figure 7; the theoretical weight percentage is higher than the experimental one for all different sized particles. However, when supposing *S*₀ = 15.23 Å², we get an excellent fit for all the components (dotted lines in Figure 7). This means that thilates form a self-assembled monolayer on the particle surface with a larger packing density than that on the flat plane; this can be considered as a result of the substantial curvature of the gold nanoparticle surface, leading to a smaller steric hindrance for thiolate adsorption. A similar result has also been reported for the long chain thiolate modified gold particles, giving *S*₀ = 17.2 Å² for C₁₄SH and *S*₀ = 15.2 Å² for C₁₈SH, respectively.⁴⁹ The good fit between theoretical and experimental values for all the components and for different sized particles shows that the surface structure in Chart 1 is general for the particles prepared in this study.

The adsorption of water molecules on the particle surface was confirmed by the TG-DTA experiments. Parts A and B of Figure 8 show the results for 10.2-Å gold particles and pure MSA, respectively. The TG curve (Figure 8A, curve a) displays four steps of mass loss during the heating from 24 to 499 °C. In the first step (24–105 °C), the mass initially increased (42–50 °C) due to the hygroscopic nature of the particles and then decreased at a rate of 4 µg/C till 105 °C (near the boiling point of water). After

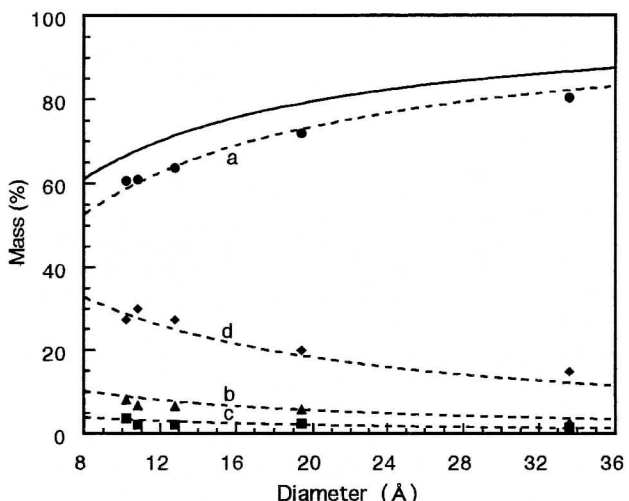


Figure 7. Comparison of the experimentally obtained weight percentages (points) with the theoretically calculated ones (broken lines) of different components for gold nanoparticles: (a) Au; (b) Na; (c) H₂O; (d) organics. The experimental data for Au, Na, and H₂O are from Table 1. The contents of organics are obtained by subtraction of weights. The bold line shows the theoretical fit for the weight percentage of gold assuming a packing density of thiolate on the gold surface of 21.4 Å².

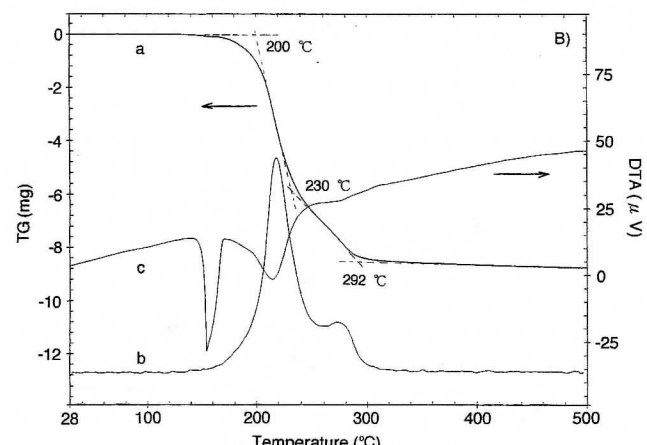
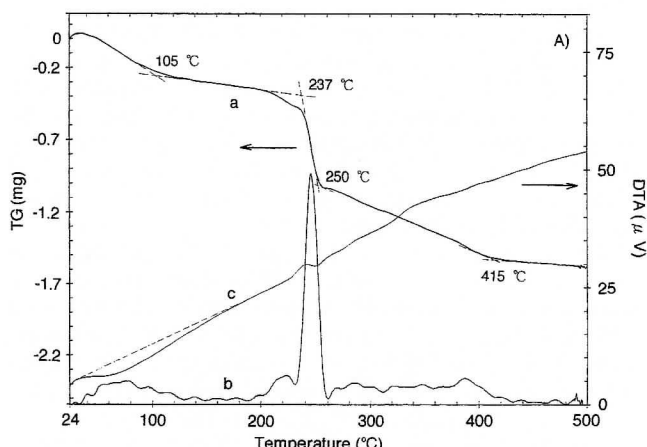


Figure 8. Thermogravimetric curve (a) and its derivative (b), as well as the differential thermoanalysis curve (c), of the 10.2 Å gold particles (A) and pure MSA (B).

that the mass continued to decrease but with a slow rate of 0.8 µg/C till 210 °C. These two mass loss steps are caused by the loss of water, because no mass loss was observed until 150 °C for the pure MSA (see Figure 8B, curve a). The evaporation of water resulted in a very broad endothermic peak centered at 50 °C in the DTA curve

(47) Sellers, H.; Ulman, A.; Schnidman, Y.; Eilers, J. E. *J. Am. Chem. Soc.* **1993**, *115*, 9389–9401.

(48) Camillone, N., III; Chidsey, C. E. D.; Liu, G.; Putvinski, T. M.; Scoles, G. *J. Chem. Phys.* **1991**, *94*, 8493–8502.

(49) Badia, A.; Singh, S.; Demers, L.; Cuccia, L.; Brown, G. R.; Lennox, R. B. *Chem. Eur. J.* **1996**, *2*, 359–363.

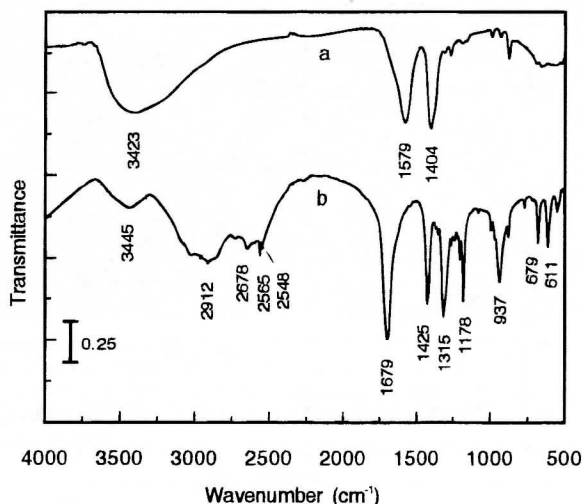


Figure 9. FT-IR spectra of carboxylate group-derivatized 10.2-Å gold particles (a) and pure MSA (b).

(Figure 8A, curve c). The mass percentage of water determined in this manner for different sized gold particles was shown in Table 1, which is in good agreement with the calculated values based on the structures in Chart 1 (Figure 7c).

Continued heating from 210 to 420 °C results in an abrupt (237–250 °C, 61 µg/C) and a subsequent slow (250–415 °C, 3.4 µg/C) mass loss due to the decomposition of the organics. However, the total mass loss during these two processes (11.8%) is much less than that of the total organic content (27.3%). This means that more than half of the organics remain in the residues. Similar results were found for other sized gold particles (see Table 1). EDAX analysis shows that S, C, and O still existed in the residues. The TG curve of pure MSA shows two steps of decomposition (Figure 8B, curves a and b). The first step (160–230 °C, 177 µg/C) amounts to 64% of the total mass, corresponding to the loss of two carboxylic acid groups (60% of the total mass). The second step occurred with a slower rate of 47 µg/C (230–292 °C). The total mass loss of these two steps amounts to 94%, showing that most of the pure organics can be removed by heating. The DTA curve (Figure 8B, curve c) displayed three peaks at 155, 210, and 280 °C. The first one was caused by the melting of MSA, and no mass loss was observed (the melting point of MSA is 153 °C). In summary, compared to the case of pure MSA, for the organics on the particle surface, (i) the starting decomposition temperature is higher, (ii) the decomposition rate of each step is slower, and (iii) the relative decomposed amount is smaller. All these findings can be explained according to the strong interaction of the organic moiety through the mercapto groups on the gold particle surface.

The structure shown in Chart 1 was further confirmed by comparison of the FT-IR spectra of gold particles with that of pure MSA, as shown in Figure 9. The spectrum of MSA is similar to the standard one.⁵⁰ The small peak at 2548 cm⁻¹, which corresponds to the S-H stretching vibration mode, disappears when the MSA molecules adsorb on the gold particle surface (compare spectra b and a), giving strong evidence that MSA anchors on the gold surface through the sulfur atom in the mercapto group. The position of one strong peak at 1679 cm⁻¹ (in the range 1680–1720 cm⁻¹) in curve b which belongs to the carbonyl stretching vibrations clearly indicates that

pure MSA molecules exist in the form of dimers. In contrast, the double peaks of the carboxylate vibration at 1579 cm⁻¹ (in the range 1540–1650 cm⁻¹, asymmetric) and 1404 cm⁻¹ (in the range 1360–1450 cm⁻¹, symmetric) in the spectra of gold particles show that the organics exist as carboxyl salts on the particle surface (curve a).^{51a} The peak position of this doublet is similar to that observed for other mercapto carboxylate salts.⁵² For the MSA molecules, hydrogen in the carboxylic acid is featured by the broad carboxylic acid O-H stretching band centered near 3000 cm⁻¹, which is superimposed on the C-H stretching bands (2800–3100 cm⁻¹). A distinctive shoulder at 2678 cm⁻¹ is due to overtones and combinations of the 1315 and 1425 cm⁻¹ bands, which are caused by the interacting C-O stretch and in-plane C-O-H deformation vibrations.^{51b,53,54} The peak at 937 cm⁻¹ (in the range 875–960 cm⁻¹) is characteristic of the out-of-plane O-H bending mode in an intermolecular hydrogen-bonding dimer structure. The strong peak at 1178 cm⁻¹ involves interacting in-plane O-H deformation and C-O stretching modes.^{51c} These peaks all disappeared after the MSA molecules adsorbed on the gold particle surface, consistent with the result that the carboxylic hydrogen was dissociated and the MSA existed in the form of a carboxyl anion. Another feature of the gold particles is the presence of a broad band in the range 2700–3700 cm⁻¹ centered at 3423 cm⁻¹; it even masked the vibration mode of the methylene group near 3000 cm⁻¹. This band is due to the various O-H stretching vibrations. It clearly confirmed the existence of water molecules in the particle surface and, possibly the O-H...O hydrogen-bonding interaction as suggested in Chart 1.

Surface Properties of Particles. Since the particle surface is covered with carboxylate anions, it is expected that the particle surface should be negatively charged. To confirm this, ζ -potential and dynamic light-scattering measurements were conducted with the 10.2-Å gold particles suspended in water. The concentration of the suspension was 4.4 mg/mL. The scattering light intensity of the freshly prepared samples was very weak and the ζ -potential cannot be detected, since the size of the particles is smaller than the detection limit of the instrument (~ 5 nm). However, after keeping the sample in ambient conditions for 4 days, scattering light from the suspension became stronger, indicating that larger aggregates of the gold particles should be generated. The average ζ -potential of these aggregates was determined to be -45.3 mV (with four measurements; electrophoretic mobility $u = -3.32 \times 10^{-4} \text{ cm}^2/(\text{V s})$), clearly showing that the surface of the aggregates was negatively charged. The dynamic light-scattering experiments indicated that there exist at least three size ranges centered at 43, 98, and 739 nm. In the solution state, the aggregates were found to be very unstable, since, after 13 days of aging, the dynamic sizes of the aggregates changed to be 122 and 661 nm and the ζ -potential of the suspension changed to -25.8 mV (u

(51) Colthup, N. B.; Daly, L. H.; Wiberley, S. E. *Introduction to Infrared and Raman Spectroscopy*, 3rd ed.; Academic Press: San Diego, CA, 1990; (a) p 291; (b) p 313; (c) p 315.

(52) Two examples can be found such as mercaptoacetic acid, sodiuim salt (ref 50, p 548), and sodium aurothiomalate monohydrate (ref 50, p 561), they have these two peaks at 1582 and 1399 cm⁻¹ and 1580 and 1405 cm⁻¹, respectively. The most striking feature is that the compound sodium aurothiomalate monohydrate, $\text{AuSC}_2\text{H}_5(\text{COONa})_2 \cdot \text{H}_2\text{O}$, whose structure is essentially the same as that of our gold particle surface, contains one molecule of H_2O , strongly supporting our finding from elemental analysis.

(53) Nuzzo, R. G.; Dubois, L. H.; Allara, D. L. *J. Am. Chem. Soc.* **1990**, *112*, 558–569.

(54) Sun, L.; Crook, R. M.; Ricco, A. J. *Langmuir* **1993**, *9*, 1775–1780.

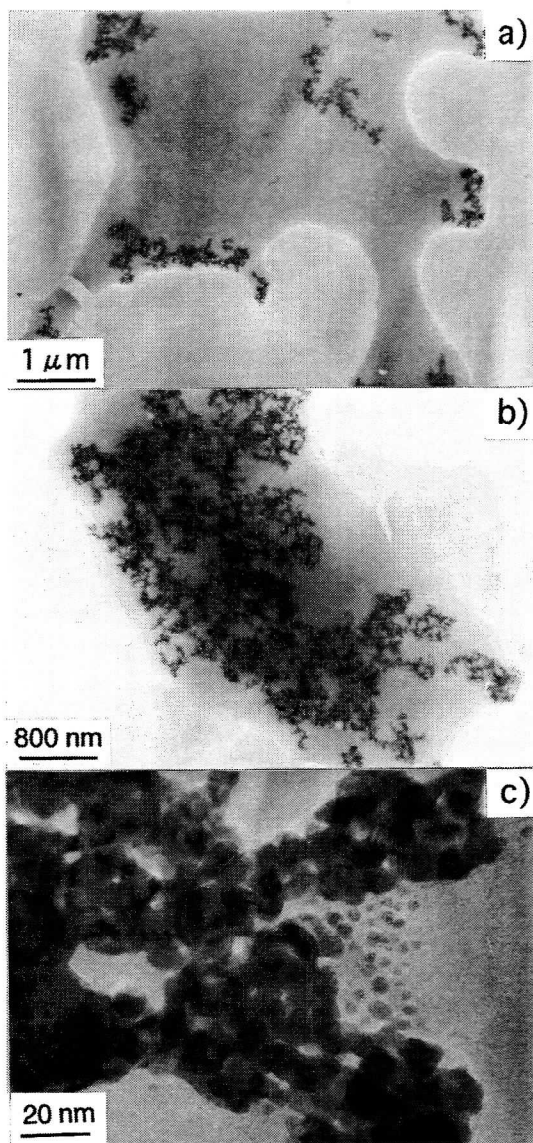


Figure 10. TEM photos of the 10.2-Å gold particles on a copper grid aged in ambient conditions for 4 days (a) and 13 days (b). The photo of part c shows a magnified part of the aggregates aged for 13 days.

$= -2.12 \times 10^{-4} \text{ cm}^2/(\text{V s})$). The largest sizes, 739 and 661 nm in both cases, are considered to be contamination. So the size of the aggregates can be said to become larger during 9 days of aging while the absolute values of the ζ -potential are lowered during this period. This conflicts with the common knowledge of the theory of electrophoresis, in which the mobility of a particle is large for a large particle, assuming a constant surface charge density. One reason for this discrepancy is the applicability of the ζ -potential concept to the charged aggregates. Physically we should rather use the electrophoretic mobility itself than the ζ -potential, as shown in the parentheses. Regardless of the above problem, it is apparent that there exists a dynamic equilibrium between the aggregates or between the particles and the aggregates. On one hand, the strong surface charges of the particles act as the repulsive force, preventing the particles from aggregation; on the other hand, the van der Waals

force between particles and hydrogen-bonding interactions from the carboxylate groups form the attraction force. Eventually, the attraction-repulsion interaction reaches an equilibrium. However, this process is dynamic, which is different from irreversible precipitation, owing to the tightly covered thiolate layer on the particle surface.

The strong interaction between the gold particles was further visualized by tracing the particle change during aging on the copper mesh (Figure 10). The specimen was prepared by dropping the suspension used for the ζ -potential measurement onto the copper mesh and then storing it in a drybox of 40% relative humidity. For the freshly prepared sample (not shown), no apparent aggregates were observed, but we do see the large area particulate monolayer, as shown as background substrates in Figure 10a. After 4 days of aging, some fractal aggregates nucleated at different sites of the particulate film (Figure 10a), indicating particle growth presumably due to the strong interactions of the carboxylate groups on the particle surface. The 13-day-aged sample (Figure 10b) shows larger area fractal structures, implying a diffusion-controlled growth mode even in the dried state. Figure 10c gives an enlarged part of the 13-day-aged aggregates; it can be seen that the fractal component is actually composed of subaggregates with the size of around 8 nm. It should be pointed out that this aggregate is very sensitive to electron beam irradiation. Although this fractal growth mode of particles may be different from that of particle growth in a suspension state, it does show that interaction between the particles is apparent due to the modification of carboxylate groups and that H_2O molecules play an important role in inducing the aggregation. In fact, in the powder state, the particle is very stable, as no apparent change can be observed from the XRD patterns even after storing in ambient conditions for more than 6 months.

Conclusions

A novel single-phase synthetic route for the generation of carboxylate-modified gold nanoparticles with sizes from 1.0 to 3.4 nm was developed. Different from the other long chain thiolate-stabilized gold particles, the small molecule mercaptosuccinic acid-stabilized gold particles are easily dispersible in water, and their dispersibility is pH-dependent. This property practically shows that these particles have a promising future in cell biology as electron microscopy markers. A large part of the particles were found to have the morphology of the truncated octahedron structure. The combined studies with elemental analysis, TG-DTA, FTIR, and ζ -potential measurements clearly show that mercaptosuccinic acid on the particle surface exists in the form of the sodium carboxylate and that, further, one H_2O molecule combines with the salt.

Acknowledgment. This work was supported in part by Grants-in-aid for Scientific Research on Basic Research (A: 09304068) and for JSPS fellows from Ministry of Education, Science, Sports and Culture, Japan. S.C. thanks the Japan Society for Promotion of Science for granting the postdoctoral fellowship. We thank Dr. T. Ida for help with the XRD experiment and Prof. K. Toriumi and Dr. Y. Ozawa for help with the thermogravimetric analysis.